Electronic supplementary materials *Mendeleev Commun.*, 2023, **33**, 631–634

2-Thienyl-substituted 3a,6a-diaza-1,4-diphosphapentalene: synthesis and complexation with 1,2,4,5-tetracyanobenzene

Matvey D. Grishin, Natalia V. Zolotareva, Yuliya S. Panova, Vyacheslav V. Sushev, Roman V. Rumyantcev, Georgy K. Fukin and Alexander N. Kornev

Table of Contents

General Remarks S2
Cyclic Voltammetry S2
X-ray Crystallography S2
Synthesis S3
Figure S1. Molecular structures of **5** S4
Figure S2. Molecular structures of **6** S5
Figure S3. Fragment of the crystal packing of **7** S5
Figure S4. Inter-stack short contacts in crystal **8** S6
Figure S5. Relative arrangement of layers of molecules in crystal **8** . . . S6
Figure S6. Theoretical molecular graph of the crystal packing fragment of the complex **8**. S7
Table S1. The main topological characteristics of the electron density in **8** . . S7
Figure S7. The region of C-H and C≡N stretching vibrations for TCNB and **8** . . S8
Figure S8. The region of deformation vibrations for TCNB and **8** S8
Figure S9. Optical absorption spectrum of **6** in CH_2Cl_2. . . . . S9
Figure S10. UV/VIS spectra of complex **8** in CH_2Cl_2 at 293 K. S9
Figure S11. Optical absorption spectrum of **7** in CH_2Cl_2. . . . . S10
Figure 12. UV/VIS spectra of complex **8** in Nujol at 293 K S10
NMR Spectra S11-S15
Figure S13. Differential scanning calorimetry of **5** S16
Figure S14. Differential scanning calorimetry of **6** S16
Figure S15. Differential scanning calorimetry of **7** S17
Figure S16. Differential scanning calorimetry of **8** S17
Theoretical electron density S18
References S18

General Remarks

All manipulations for the synthesis, isolation, and sample preparation for physicochemical studies were carried out *in vacuo* and under a high-purity argon atmosphere using the Schlenk technique. All reagents and solvents were obtained from commercial sources and dried by using standard procedures before use. The ^{1}H, ^{13}C, and ^{31}P NMR spectra were measured on a Bruker AV 300 and Bruker AV 400 instruments at 298 K. The IR spectra of the synthesized compounds were recorded on a FSM 1201 in the range from 4000 to 400 cm^{-1}. The *absorption spectra* were recorded with a Perkin-Elmer Lambda 25 spectrometer. The *elemental analysis* was performed on a Vario EL cube automatic CHNS elemental analyzer (Elementar Analysen systeme GmbH) using helium (6.0 grade) as the carrier gas. The content of P was determined from the dry residue during pyrolysis with a gravimetric completion, the content of halogen was determined during pyrolysis with a silver grid. *Mass chromatograms* were recorded on a Polaris Q/Trace GC Ultra chromatographic mass spectrometer with a TR-5MS capillary chromatographic column 60 m long and 0.25 mm in diameter at an ionizing electron energy of 70 eV in the mass number range of 40-700. *Differential Scanning Calorimetry* study was performed in the temperature range of 20-300 °C with a DSC204F1 Phoenix differential scanning calorimeter (Netzsch Geratebau, Germany). The reliability of the operation of the calorimeter was tested using standard calibration experiments for measurements of thermodynamic characteristics of the melting of n-heptane, mercury, indium, tin, lead, bismuth, and zinc. The calorimetric measurements of the complexes were carried out in a highly pure nitrogen atmosphere at a heating rate of $10^{o}C \cdot min^{-1}$.

Cyclic Voltammetry

Electrochemical behavior of the compounds has been investigated using the Corrtest CS300 potentiostat/galvanostat (China) equipped with standard three electrode cell. Glassy carbon disk (1 mm) was used as working electrode, a non-aqueous $Ag/AgNO_3$ was served as reference electrode, and a Pt wire as the counter electrode. 0.1 M $[Bu_4N][PF_6]$ was used as supporting electrolyte. All electrochemical measurements were carried out under Ar atmosphere at a scan rate 100 mV s^{-1}.

X-ray Crystallography

The X-ray diffraction data for complexes **5**–**8** were collected on a Rigaku OD Xcalibur E diffractometer (MoKα radiation, ω-scan technique, λ = 0.71073 Å). The intensity data for all compounds were integrated by CrysAlisPro program [S1]. An absorption correction was introduced by SCALE3 ABSPACK algorithm. All structures were solved by dual method [S2] and refined on F_{hkl}^2 using SHELXTL package [S3]. All non-hydrogen atoms were refined anisotropically. All hydrogen atoms were refined using a riding model ($U_{iso}(H) = 1.5U_{eq}(C)$ for CH_3-group and $U_{iso}(H) = 1.2U_{eq}(C)$ for other groups). The structures **6** and **8** exhibit disorder of the 2-thiophen-2-yl substituents. Identical anisotropic displacement parameters for pairs of disordered atoms were received with EADP instruction. SADI, DFIX, SAME, FLAT and ISOR instructions were used to refine disordered fragments of molecules. The structure of **8** was refined as a two-component non-merohedral twin using the HKLF5 format data file; the twin ratio refined to 0.61/0.39.

CCDC 2255159-2255162 (**5-8**) contain the supplementary crystallographic data for this paper. These data can be obtained free of charge from The Cambridge Crystallographic Data Centre *via* http://www.ccdc.cam.ac.uk.

Synthesis

(*1E,2E*)-1,2-Bis[1-(2-thienyl)propylidene]hydrazine (5).

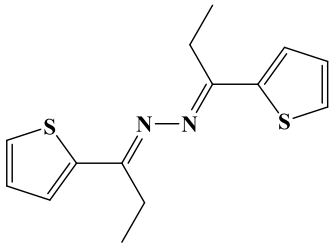

Hydrazine hydrate (1.9 ml, 0.04 mol) was added to a solution of 1-(2-thienyl)propan-1-one (11.24 g, 0.08 mol) and HOAc (0.2 ml, 3.0 mmol) in ethanol (20 ml). The reaction mixture was stirred under reflux for 6 hours. The azine solid was separated out on cooling, dried under vacuum and recrystallized from hexane. Yield 8.3 g (75%), yellow crystals. Found (%): C, 60.79; H, 5.85; N, 10.12; S, 23.24. Calc. for $C_{14}H_{16}N_2S_2$ (%): C, 60.83; H, 5.83; N, 10.14; S, 23.20. **IR** (Nujol, ν, cm^{-1}): 3096 w, 3068 w, 1887 w, 1810 w, 1744 w, 1685 w, 1573 s, 1518 w, 1421 m, 1350 w, 1286 w, 1233 m, 1057 s, 998 w, 911 s, 850 s, 795 m, 744 w, 613 m, 468 m. **^{1}H NMR** (300 MHz, C_6D_6, δ, ppm, *J*, Hz): 1.10 (t, $^3J_{H,H}$ = 7.6, 6H, *C*H_3); 2.89 (q, $^3J_{H,H}$ = 7.6, 4H, *C*H_2); 6.60 – 7.07 (m, 6H, **tph** = thiophene ring). **^{13}C NMR** (75 MHz, C_6D_6, δ, ppm): 12.11 (s, CH_3), 22.55 (s, CH_2), 127.15 (s, tph); 127.34 (s, tph); 128.74(s, tph); 144.21(s, C_{ipso}, tph); 162.92 (s, *C*=N). **MS** (EI, 70 eV), *m/z* (I_{rel} (%)): 276.1 $[M]^+$ (35); 247.1 $[M\text{-}Et]^+$ (100); 166.2 [M-Et, $-C_4H_3S]^+$ (75); 138.2 $[M/2]^+$ (40). **DSC** (10°C/min): m.p. 105 °C; T_{dec} > 222 °C.

1,4-Dichloro-2,5-dimethyl-3,6-di(2-thienyl)-3a,6a-diaza-1,4-diphosphapentalene (**6**).

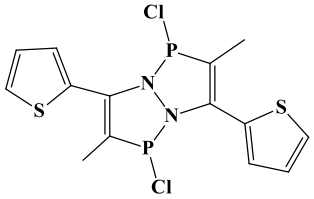

Phosphorus trichloride (1.0 g, 7.2 mmol) was added dropwise to azine **5** (1.0 g, 3.6 mmol) in an argon atmosphere. The reaction mixture was heated at 80°C for 3.5 h until the end of the release of HCl. The resulting solid was washed with dichloromethane and recrystallized from THF. Yield 0.95 g (65%), yellow crystals. Found (%): C, 41.52; H, 3.05; N, 6.86; P, 15.25. Calc. for $C_{14}H_{12}Cl_2N_2P_2S_2$ (%): C, 41.49; H, 2.98; N, 6.91; P, 15.29. **IR** (Nujol, ν, cm^{-1}): 3089 w, 1576 s, 1502 m, 1422 w, 1367 m, 1350 m, 1315 m, 1293 m, 1233 m, 1173 s, 1123 m, 1082 w, 1051 m, 993 w, 979 m, 880 m, 849 m, 756 m, 744 m, 652 w, 640 w, 611 w, 501 w, 490 w, 470 w, 450 m. **^{1}H NMR** (300 MHz, CD_2Cl_2, δ, ppm, *J*, Hz): 2.18 (m, 6H, CH_3), 7.26 (m, 2H, tph), 7.52 (m, 2H, tph), 7.66 (m, 2H, tph). **^{1}H{^{31}P} NMR** (300 MHz, CD_2Cl_2, δ, ppm, *J*, Hz): 2.19 (s, 6H, 2 CH_3), 7.26 (m, 2H, tph), 7.52 (m, 2H, tph), 7.66 (m, 2H tph). **^{13}C{^{1}H}** (75 MHz, d_8-THF, δ, ppm): 10.7-11.7 (m, CH_3), 116.7-117.3 (m, *C*P), 127.5-127.6 (m, tph), 128.6 (s, tph), 129.3-129.8 (m, tph), 130.8-131.8 (m, tph), 138.52 (s, CN). **^{31}P{^{1}H}** (81 MHz, d_8-THF, δ, ppm): 114.6 (s), 118.7 (s). **MS** (EI, 70 eV), *m/z* (I_{rel} (%)): 403.98 $[M]^+$ (10), 369.16 $[M\text{-}Cl]^+$ (40), 334.19 $[M\text{-}2Cl]^+$ (100). **UV-vis**, λ_{max}/nm: (CH_2Cl_2): 270, 360. **DSC** (10°C/min): m.p. 216 °C; T_{dec} > 250 °C.

2,5-Dimethyl-3,6-di(2-thienyl)-3a,6a-diaza-1,4-diphosphapentalene (**7**).

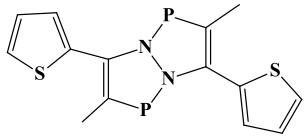

A solution of dichloride **6** (0.41 g, 1.0 mmol) in THF (20 ml) was added to an excess of vacuum preheated magnesium powder (0.11 g, 4.5 mmol). The suspension was stirred for 8 h. During the reaction, the colour of the solution turned dark red, then burgundy. The solvent (THF) was replaced with toluene; $MgCl_2$ was filtered off, the solution was concentrated. The precipitated burgundy crystals were recrystallized from THF. Yield 0.28 g, 83%. Found (%): C, 50.32; H, 3.65; N, 8.35; P, 18.48; S, 19.22; Calc. for $C_{14}H_{12}N_2P_2S_2$ (%): C, 50.29; H, 3.62; N, 8.38; P, 18.53; S, 19.18. **^{1}H NMR** (400 MHz, d_8-THF, δ, ppm, *J*, Hz): 2.5 (d, $^3J_{H,P}$ = 13.9, 6H, CH_3), 7.24 – 7.65 (m, 6H, tph). **^{13}C{^{1}H}** (100 MHz, d_8-THF, δ, ppm): 11.74 (d, $^2J_{CP}$ = 29.4, *C*H_3), 125.1 (dd, *J* = 7.6, 2.7, *C*N), 125.9 (d, *J* = 3.1, tph), 127.07 (s, tph), 127.7 (d, *J* = 10, tph), 131.2 (d, *J* = 2.7,

C_{ipso}), 144.7 (dd, J = 46.2, 2.0, CP). **^{31}P{^{1}H}** (81 MHz, d_8-THF, δ, ppm): 192.15 (s). **^{31}P** (81 MHz, d_8-THF, δ, ppm, J, Hz): 192.12 (q, $^{3}J_{P,H}$ = 13.6). **IR** (Nujol, ν, cm^{-1}): 1584 m, 1300 m, 1241 w, 1230 w, 1157 m, 1063 w, 1052 w, 994 w, 974 w, 937 w, 918 w, 897 w, 837 w, 815 w, 753 w, 706 m, 691 w, 676 m, 639 w, 611 w, 569 w, 561 w, 507 w, 486 w. **MS** (EI, 70 eV), m/z (I_{rel} (%)): 334.18 $[M]^+$(100). **UV-vis**, λ_{max}/nm: (CH_2Cl_2): 260, 340, 457. **DSC** (10°C/min): m.p. 122 °C, T_{dec} > 162 °C.

Complex of 2,5-dimethyl-3,6-di(2-thienyl)-3a,6a-diaza-1,4-diphosphapentalene with 1,2,4,5-tetracyanobenzene (8): A solution of TCNB (0.178 g, 1.0 mmol) in THF (15 ml) was added to a solution of **7** (0.334 g, 1.0 mmol) in THF (20 ml). The mixture was left overnight at 0°C. Black crystals of the product **8** were filtered and dried in vacuum. Yield 0.36 g, 70 %. Found (%): C, 56.30; H, 2.79; N, 16.36; P, 12.01; S, 12.48. Calc. for $C_{24}H_{14}N_6P_2S_2$ (%): C, 56.25; H, 2.75; N, 16.40; P, 12.09; S, 12.51. **IR** (Nujol, ν, cm^{-1}): 3105 w, 3089 w, 3028 w, 2240 m, 2225 m, 1733 w, 1586 m, 1516 m, 1414 m, 1342 w, 1292 m, 1284 m, 1252 w, 1241 w, 1222 w, 1171 m, 1072 w, 1052 w, 981 w, 911 s, 863 m, 836 s, 756 m, 708 s, 636 w, 623 w, 591 w, 583 w, 568 w, 506 s, 488 m, 468 m. **DSC** (10°C/min): T_{dec} > 199.4 °C.

Figures

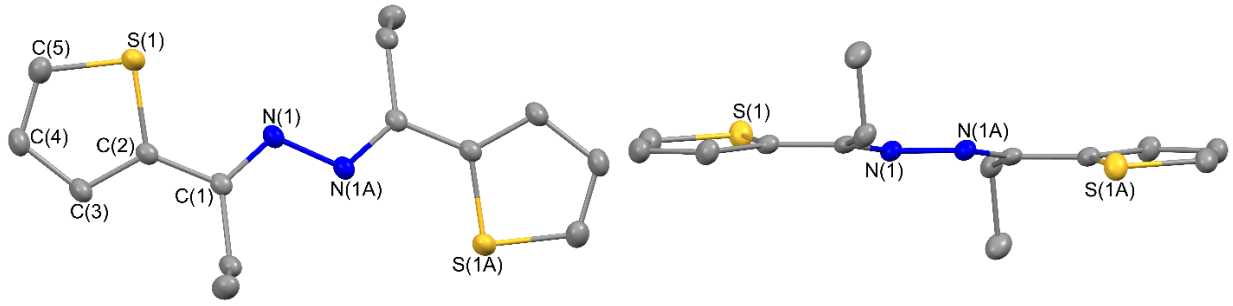

a **b**

Figure S1. Molecular structures of **5**. The top view (**a**) and side view (**b**). Thermal ellipsoids drawn at the 30% probability level. Hydrogen atoms are omitted for clarity. Selected bond lengths [Å] and angles [°]: N(1)-N(1A) 1.401(2), N(1)-C(1) 1.3005(14), S(1)-C(2) 1.7244(13), S(1)-C(5) 1.7039(14), C(1)-C(2) 1.4556(17), C(2)-C(3) 1.3756(17), C(3)-C(4) 1.4249(19), C(4)-C(5) 1.359(2); C(1)-N(1)-N(1A) 113.81(12), N(1)-C(1)-C(2) 115.63(11), C(2)-S(1)-C(5) 92.12(7). Symmetry transformations used to generate equivalent atoms (A): -x+1,-y+1,-z+1.

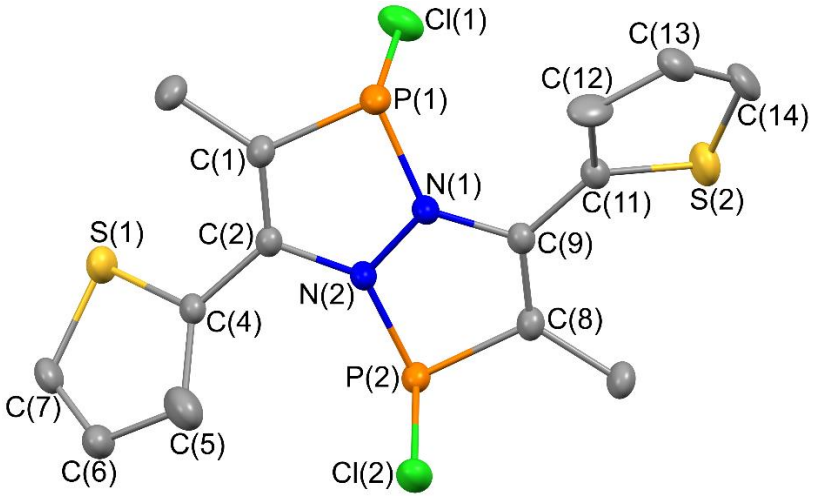

Figure S2. Molecular structures of **6**. Thermal ellipsoids drawn at the 30% probability level. Hydrogen atoms are omitted for clarity. Selected bond lengths [Å] and angles [°]: P(1)-N(1) 1.7073(17), P(1)-C(1) 1.792(2), P(1)-Cl(1) 2.1662(9), P(2)-N(2) 1.6964(17), P(2)-C(8) 1.801(2), P(2)-Cl(2) 2.1798(9), N(1)-N(2) 1.412(2), C(1)-C(2) 1.353(3), C(8)-C(9) 1.351(3); N(1)-P(1)-C(1) 88.31(9), N(1)-P(1)-Cl(1) 104.14(7), C(1)-P(1)-Cl(1) 99.46(8), N(2)-P(2)-C(8) 88.07(9), N(2)-P(2)-Cl(2) 104.80(7), C(8)-P(2)-Cl(2) 96.56(7), C(9)-N(1)-N(2) 109.26(16), C(9)-N(1)-P(1) 131.55(14), N(2)-N(1)-P(1) 113.57(13), C(2)-N(2)-N(1) 110.34(15), C(2)-N(2)-P(2) 134.23(14), N(1)-N(2)-P(2) 115.37(13).

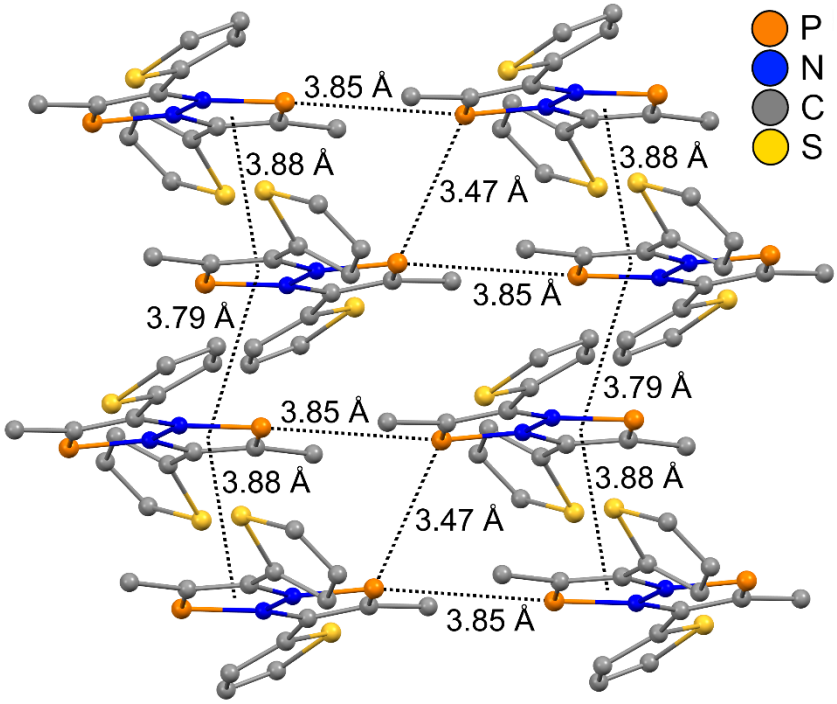

Figure S3. Fragment of the crystal packing of **7**. Hydrogen atoms are omitted for clarity.

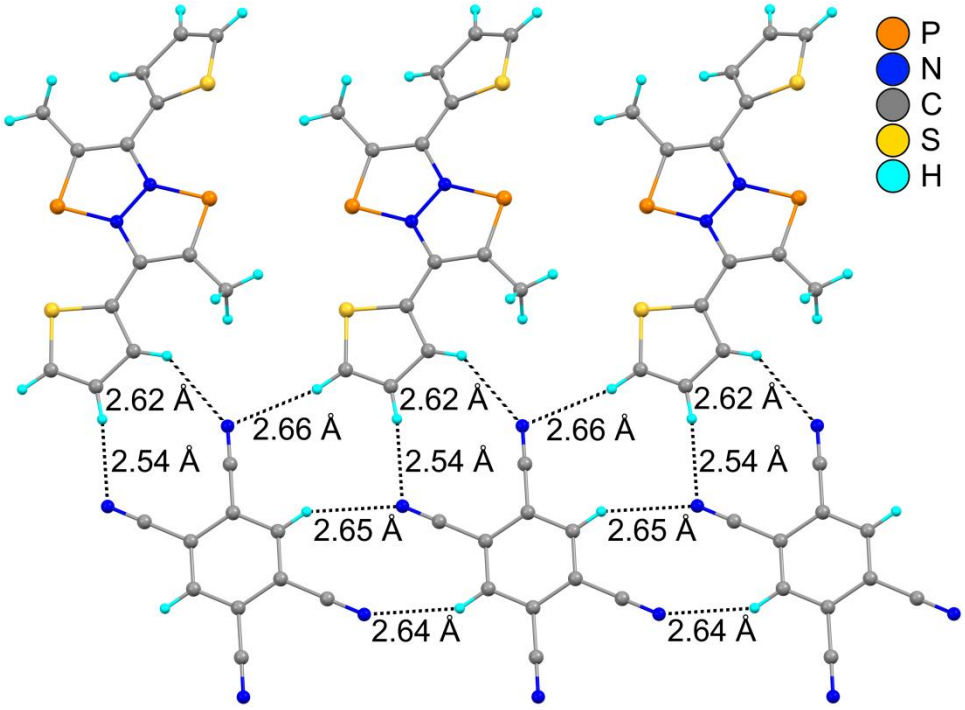

Figure S4. Inter-stack short contacts in crystal **8** between D···A and A···A molecules, lying in the same plane.

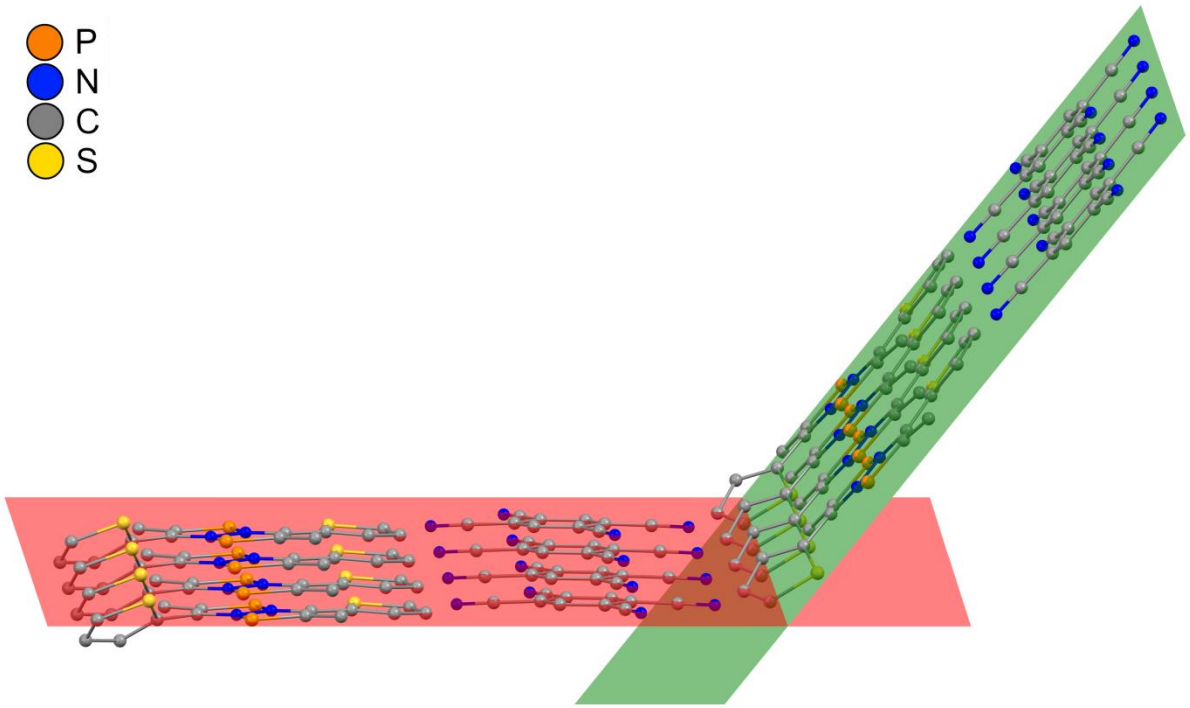

Figure S5. Relative arrangement of layers of molecules in neighboring stacks AB in crystal **8**.

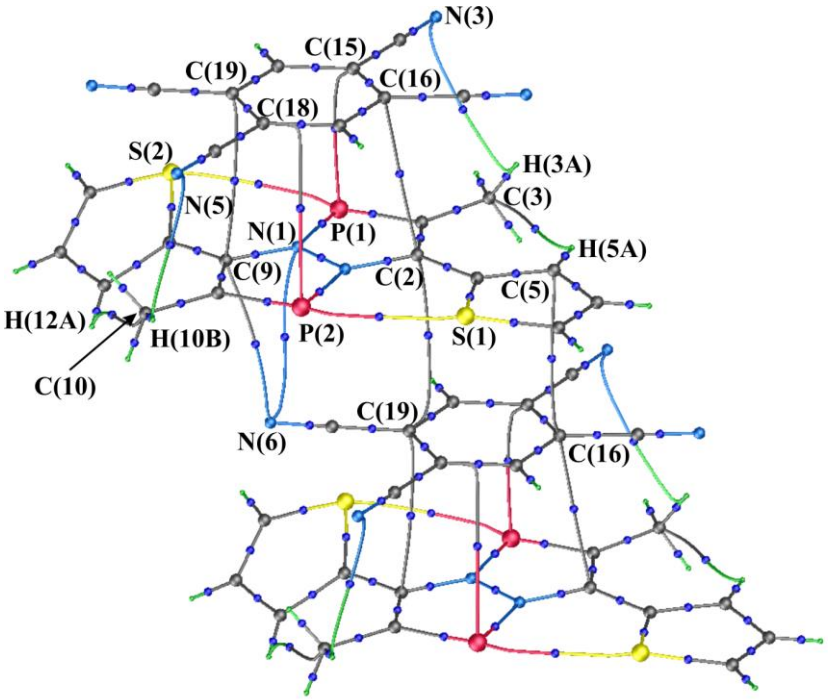

Figure S6. Theoretical molecular graph of the crystal packing fragment of the complex **8**. Only the critical points (3,-1) are given (blue color).

Table S1. The main topological characteristics of the electron density in complex **8**:

Bond	$\rho(\mathbf{r})$, a.e.	$\nabla^2\rho(\mathbf{r})$, a.e.	$v(\mathbf{r})$, a.e.	$h_e(\mathbf{r})$, a.e.
P(1)-N(1)	0.145	0.328	-0.258	-0.088
P(1)-C(1)	0.179	-0.045	-0.322	-0.167
P(2)-N(2)	0.145	0.322	-0.256	-0.088
P(2)-C(8)	0.178	-0.044	-0.320	-0.166
N(1)-N(2)	0.307	-0.002	-0.802	-0.401
N(1)-C(9)	0.300	-0.637	-0.721	-0.440
N(2)-C(2)	0.289	-0.547	-0.681	-0.409
C(15)-C(21)	0.268	-0.486	-0.598	-0.360
N(3)-C(21)	0.490	-0.780	-1.684	-0.939
N(4)-C(22)	0.494	-0.685	-1.716	-0.944
C(16)-C(22)	0.266	-0.474	-0.592	-0.355
N(5)-C(23)	0.496	-0.774	-1.718	-0.956
C(18)-C(23)	0.266	-0.477	-0.591	-0.355
C(19)-C(24)	0.269	-0.491	-0.602	-0.363
N(6)-C(24)	0.489	-0.789	-1.677	-0.937
C(1)-C(2)	0.308	-0.676	-0.749	-0.459
C(1)-C(3)	0.241	-0.375	-0.505	-0.299
C(2)-C(4)	0.269	-0.513	-0.603	-0.365
C(4)-S(1)	0.230	-0.409	-0.461	-0.282
C(4)-C(5)	0.269	-0.461	-0.606	-0.361
S(1)-C(7)	0.212	-0.307	-0.409	-0.243
C(5)-C(6)	0.293	-0.603	-0.690	-0.420
C(6)-C(7)	0.337	-0.836	-0.866	-0.538
C(8)-C(9)	0.311	-0.700	-0.763	-0.469

Bond	$\rho(\mathbf{r})$, a.e.	$\nabla^2\rho(\mathbf{r})$, a.e.	$v(\mathbf{r})$, a.e.	$h_e(\mathbf{r})$, a.e.
C(8)-C(10)	0.240	-0.374	-0.502	-0.298
C(9)-C(11)	0.269	-0.528	-0.602	-0.367
C(11)-S(2)	0.221	-0.359	-0.434	-0.262
C(11)-C(12)	0.276	-0.493	-0.630	-0.377
S(2)-C(14)	0.213	-0.313	-0.410	-0.244
C(12)-C(13)	0.249	-0.390	-0.532	-0.315
C(13)-C(14)	0.324	-0.758	-0.813	-0.501
C(15)-C(16)	0.301	-0.679	-0.721	-0.445
C(15)-C(20)	0.308	-0.699	-0.751	-0.463
C(16)-C(17)	0.310	-0.717	-0.753	-0.466
C(17)-C(18)	0.309	-0.717	-0.753	-0.466
C(18)-C(19)	0.297	-0.654	-0.703	-0.433
C(19)-C(20)	0.312	-0.721	-0.762	-0.471
P(1)…S(2)	0.015	0.029	-0.008	0.000
P(1)…C(15)	0.009	0.021	-0.004	0.001
P(2)…S(1)	0.020	0.033	-0.011	-0.002
P(2)…C(18)	0.010	0.022	-0.004	0.001
N(3)…H(3A)	0.268	0.016	-0.002	0.001
N(5)…H(10B)	0.004	0.014	-0.002	0.001
C(2)…C(16)	0.007	0.023	-0.003	0.001
C(3)…H(5A)	0.013	0.057	-0.009	0.003
C(9)…C(19)	0.006	0.019	-0.003	0.001
C(10)…H(12A)	0.011	0.044	-0.007	0.002

Infrared Spectra

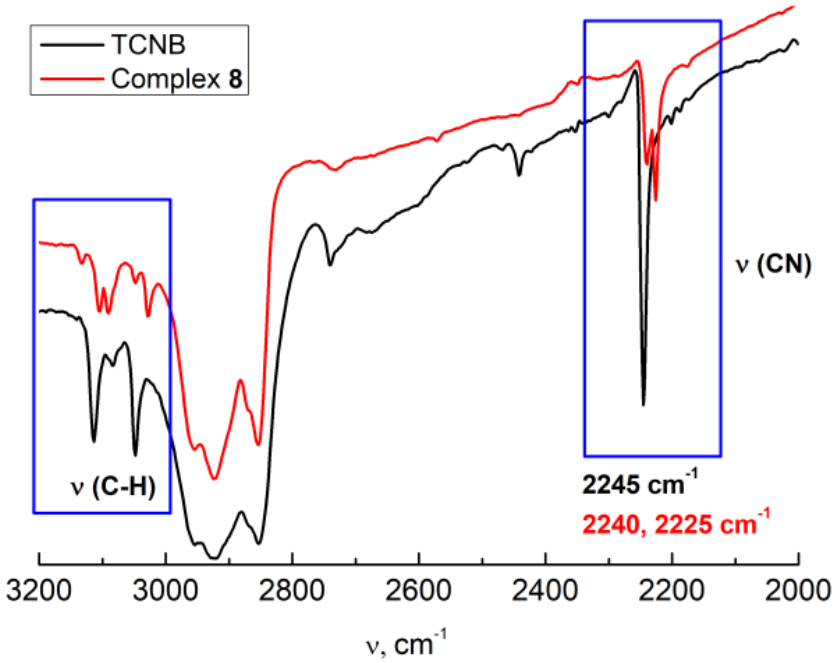

Figure S7. The region of C-H and C≡N stretching vibrations for TCNB (black) and **8** (red).

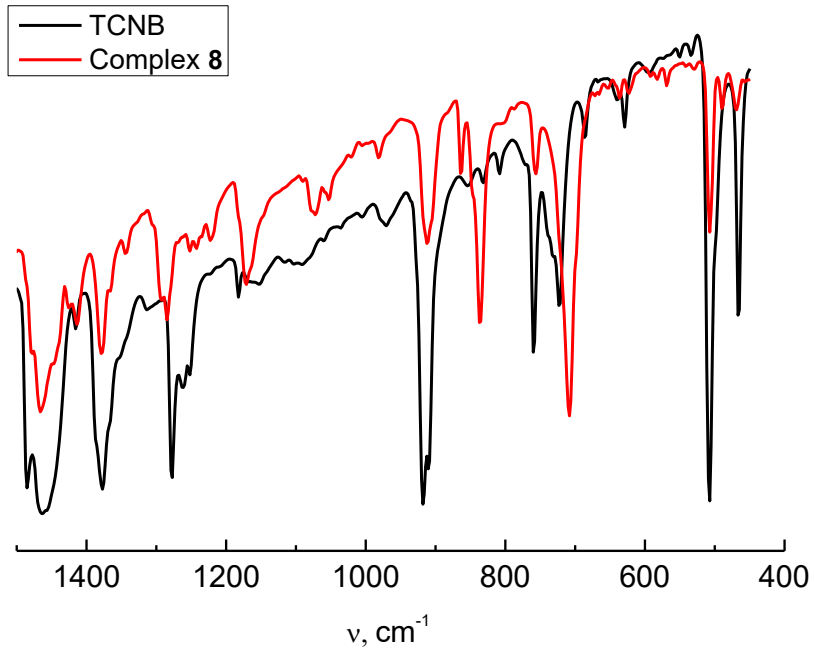

Figure S8. The region of deformation vibrations for TCNB (black) and **8** (red).

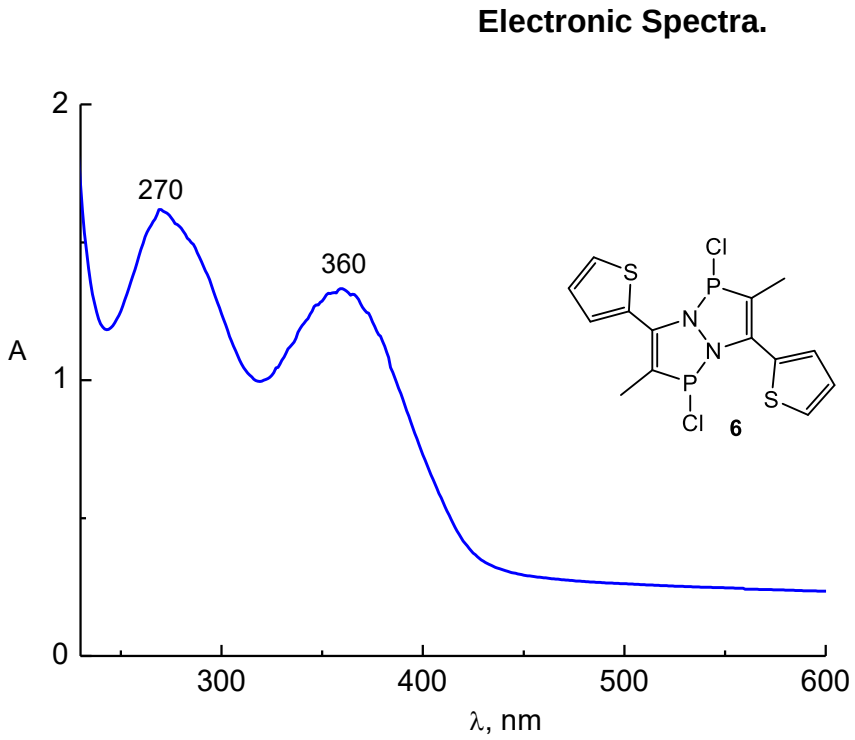

Figure S9. Optical absorption spectrum of **6** in CH_2Cl_2.

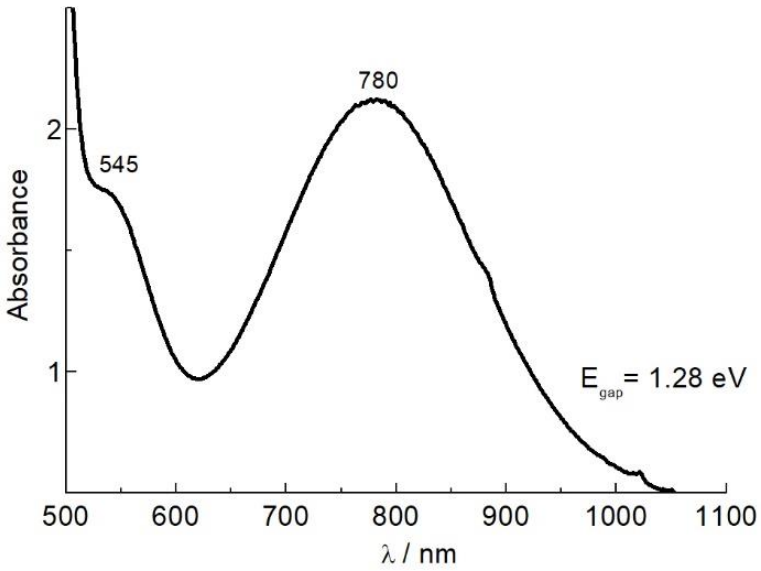

Figure S10. UV/VIS spectra of complex **8** in CH_2Cl_2 at 293 K.

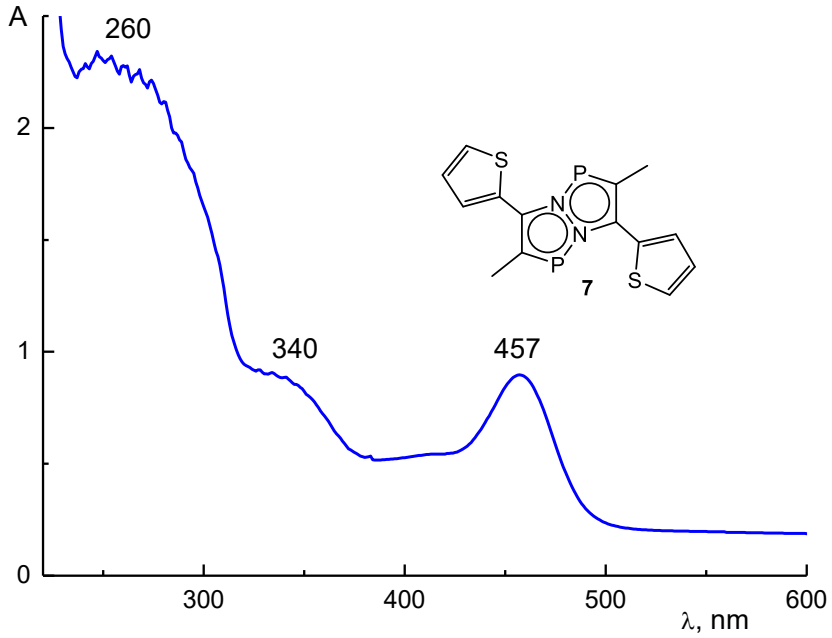

Figure S11. Optical absorption spectrum of **7** in CH_2Cl_2.

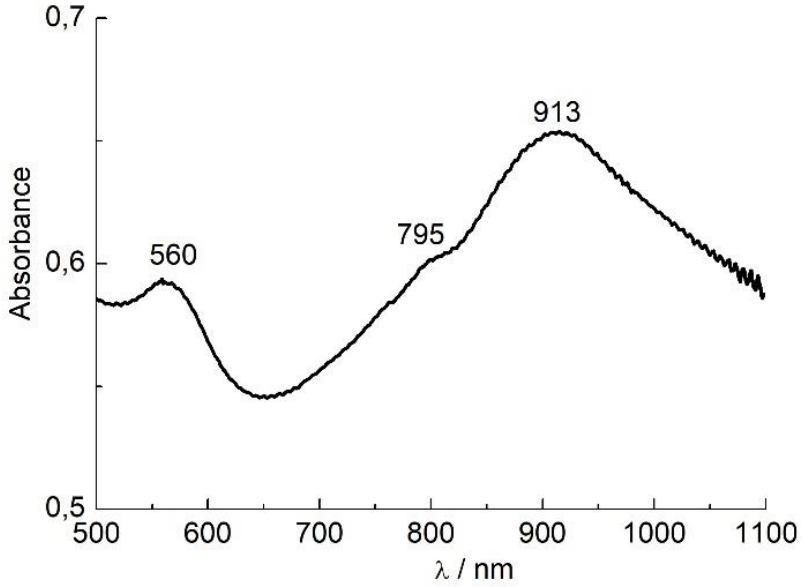

Figure S12. UV/VIS spectra of complex **8** in Nujol at 293 K.

NMR Spectra

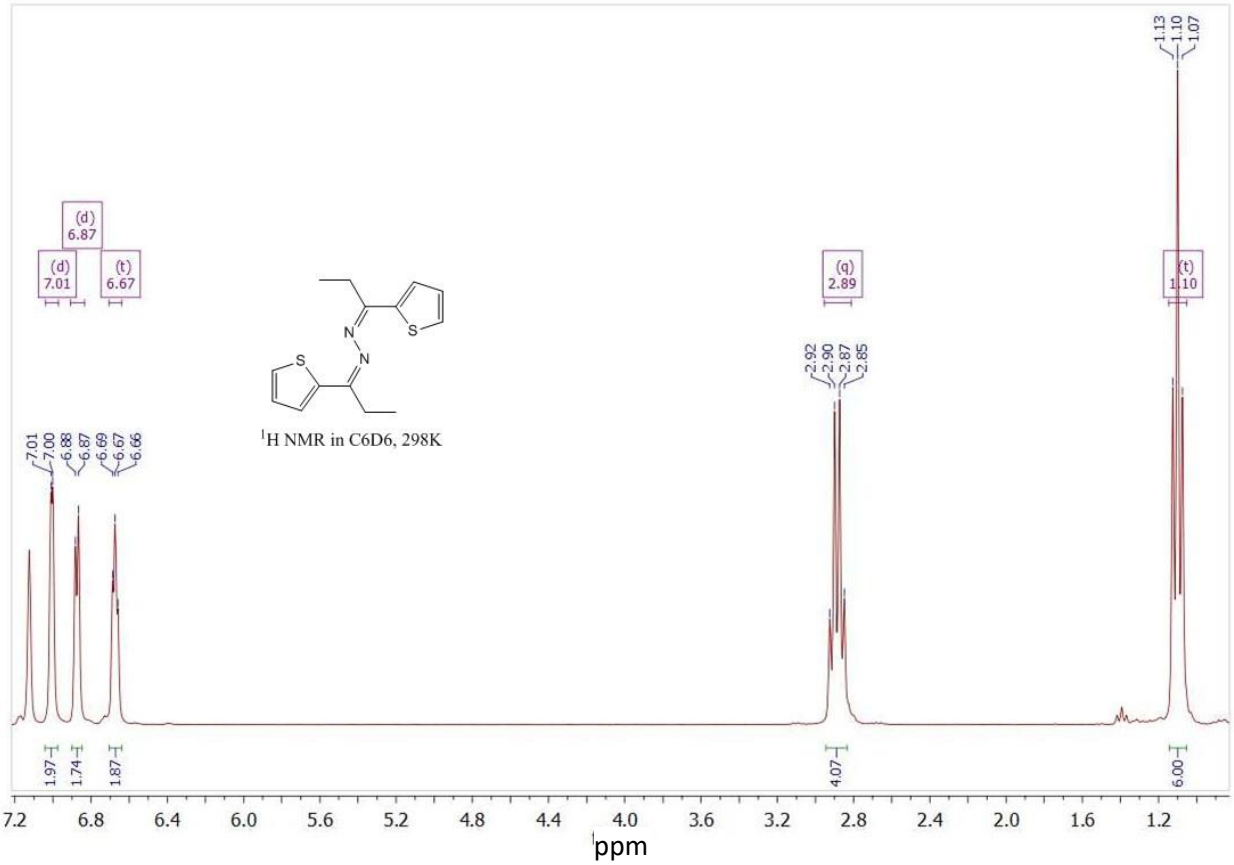

^{1}H NMR in C6D6, 298K

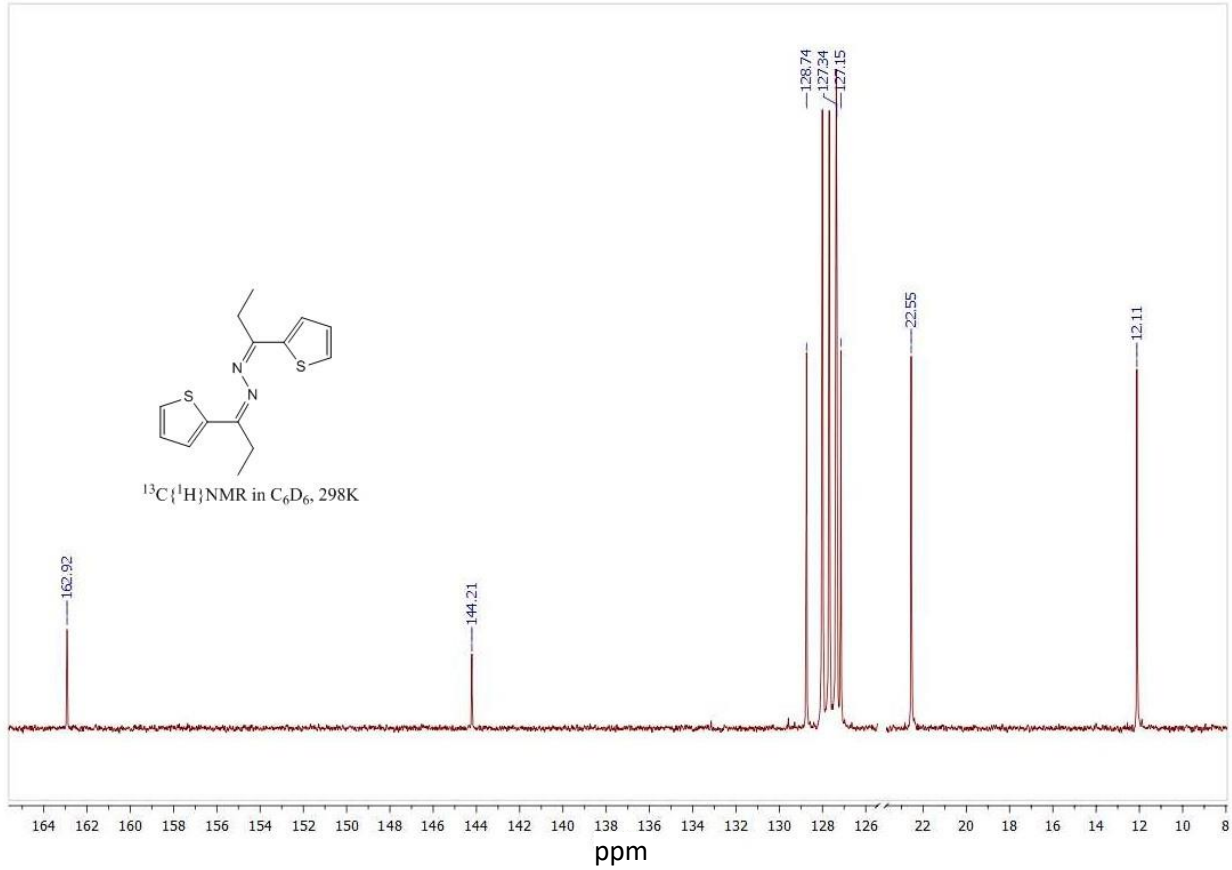

$^{13}C\{^1H\}$NMR in C_6D_6, 298K

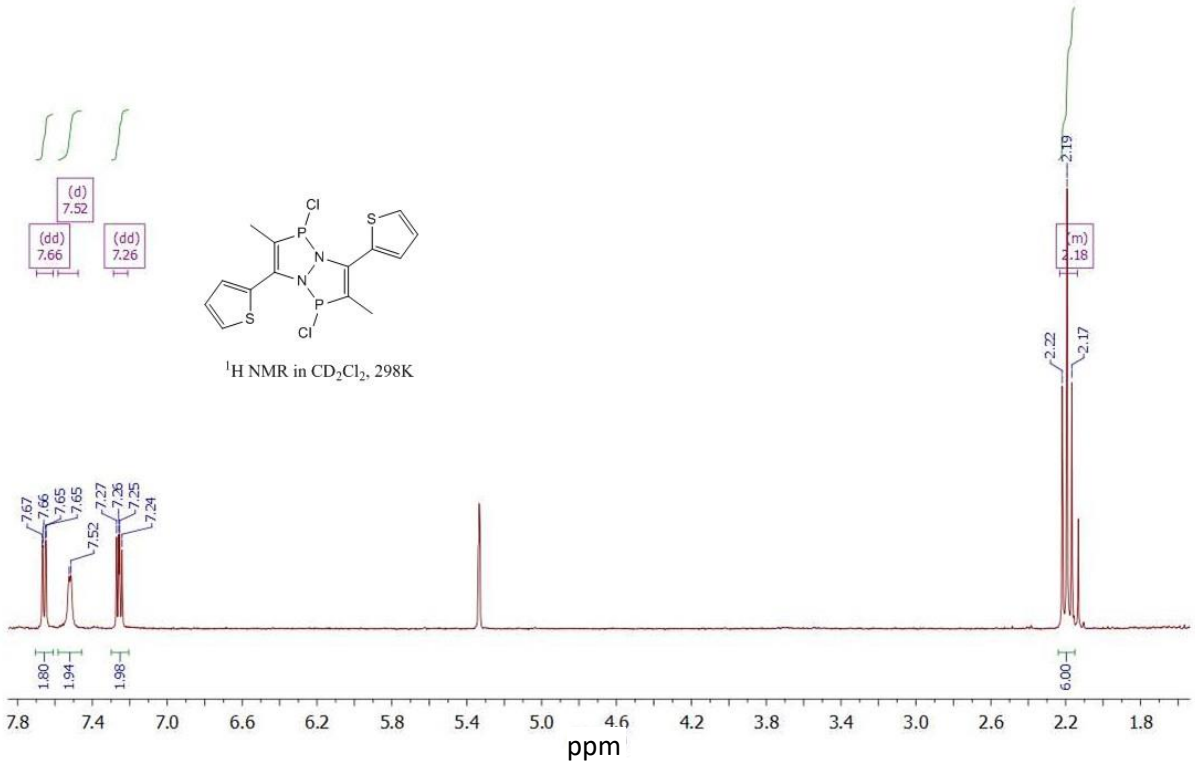

^{1}H NMR in CD_2Cl_2, 298K

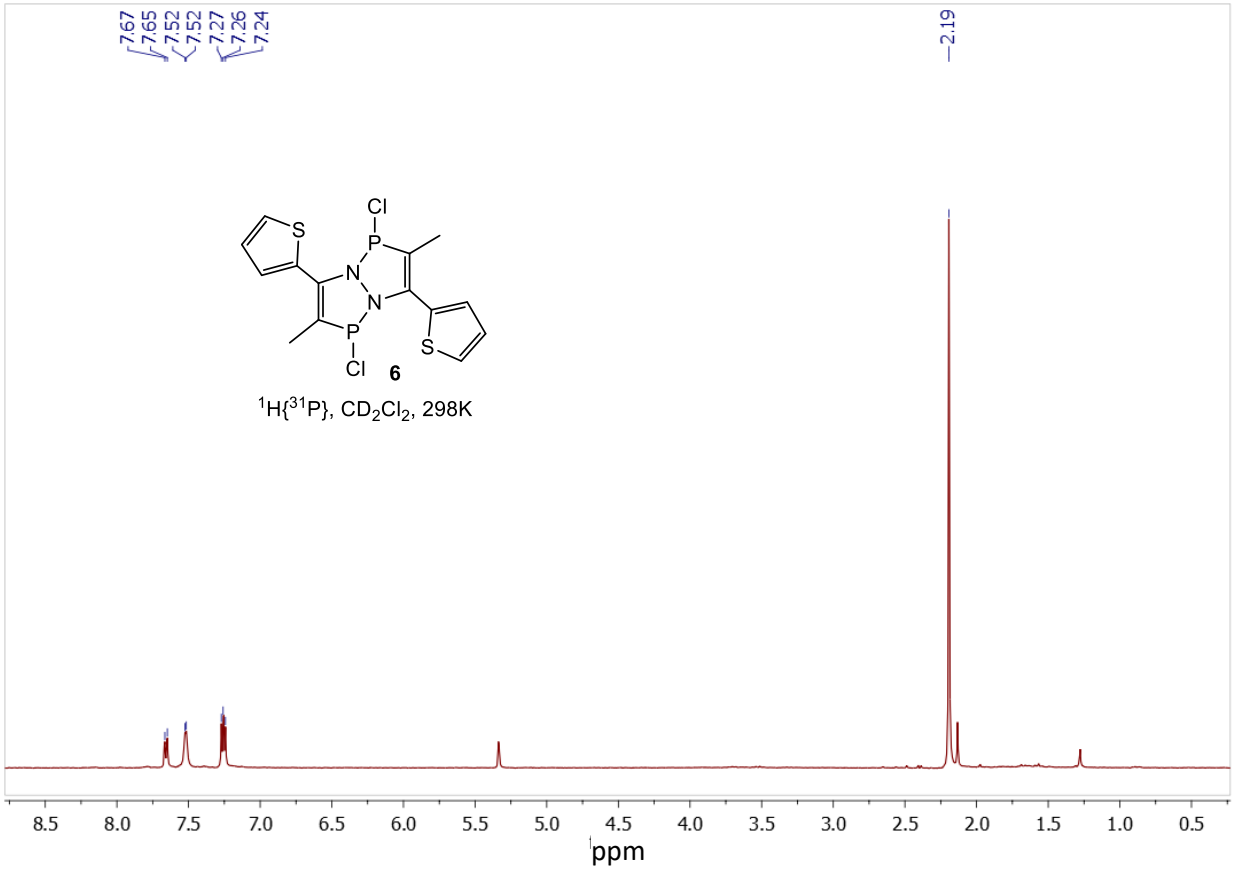

6

^{1}H{^{31}P}, CD_2Cl_2, 298K

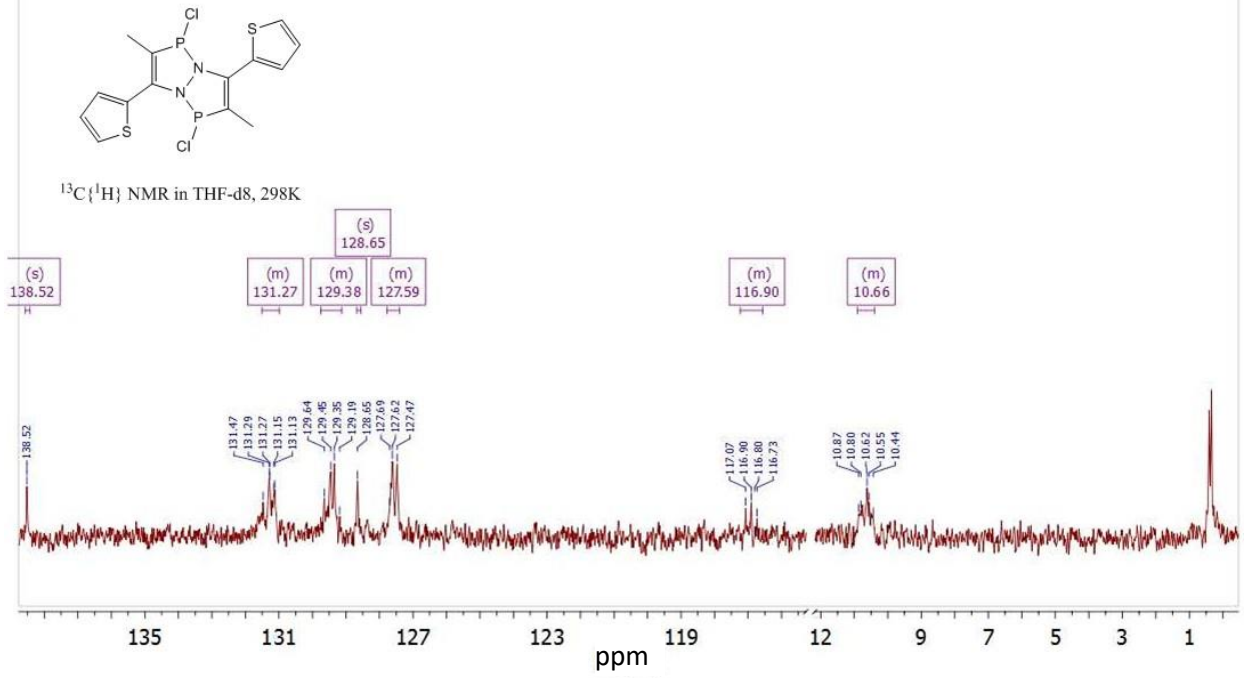
Cl
P
N
N
P
Cl
S
S
$^{13}C\{^{1}H\}$ NMR in THF-d8, 298K
(s) 138.52
(m) 131.27
(m) 129.38
(s) 128.65
(m) 127.59
(m) 116.90
(m) 10.66
138.52
131.47
131.29
131.27
131.15
131.13
129.64
129.45
129.35
129.19
128.65
127.69
127.62
127.47
117.07
116.90
116.80
116.73
10.87
10.80
10.62
10.55
10.44
135
131
127
123
119
12
9
7
5
3
1
ppm

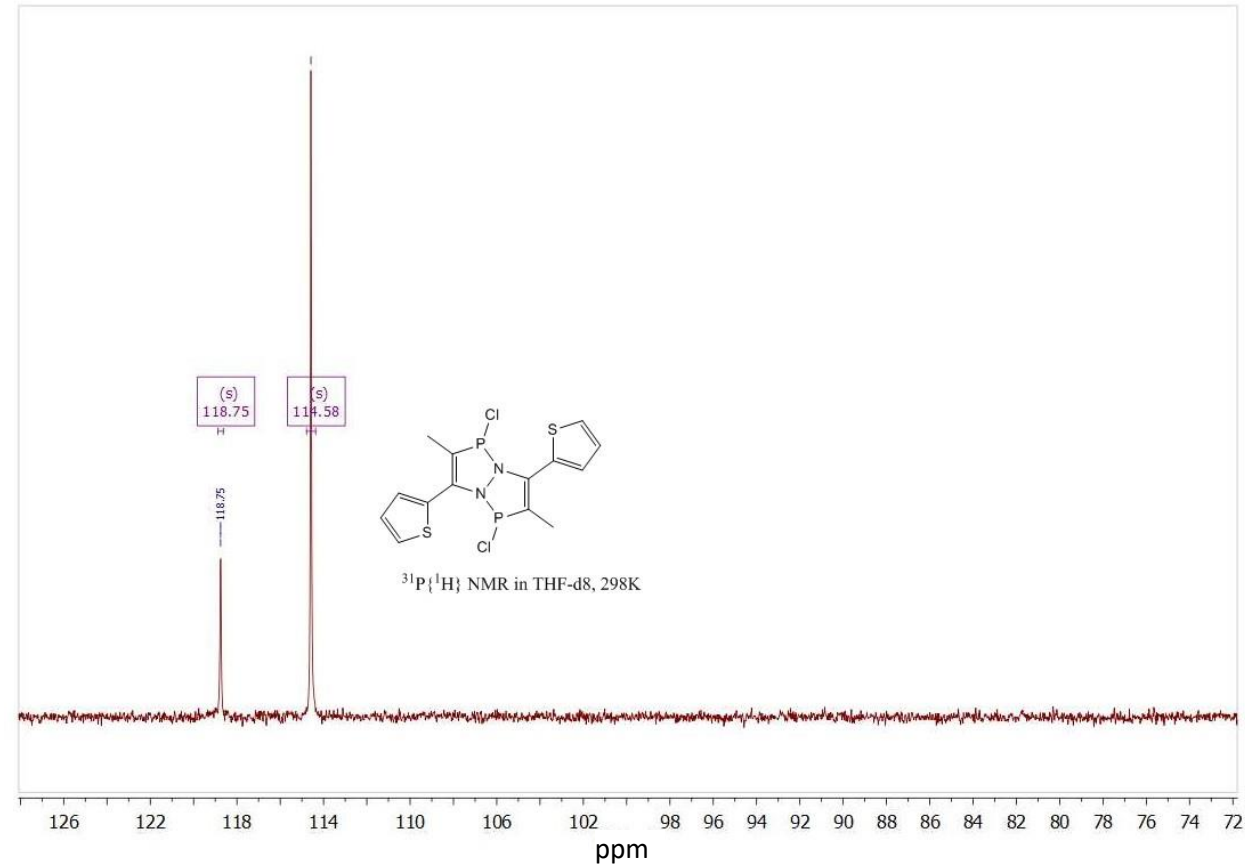
(s) 118.75
(s) 114.58
118.75
Cl
P
N
N
P
Cl
S
S
$^{31}P\{^{1}H\}$ NMR in THF-d8, 298K
126
122
118
114
110
106
102
98
96
94
92
90
88
86
84
82
80
78
76
74
72
ppm

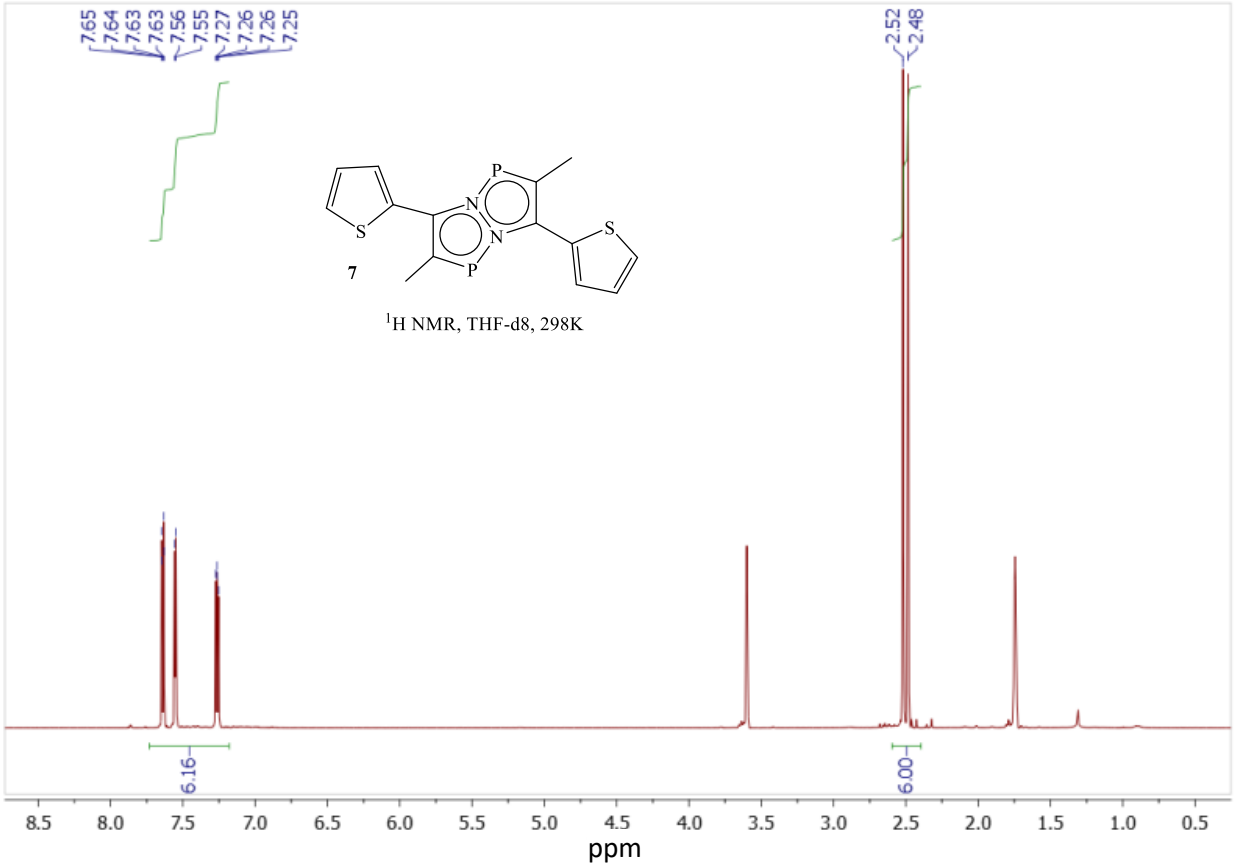

^{1}H NMR, THF-d8, 298K

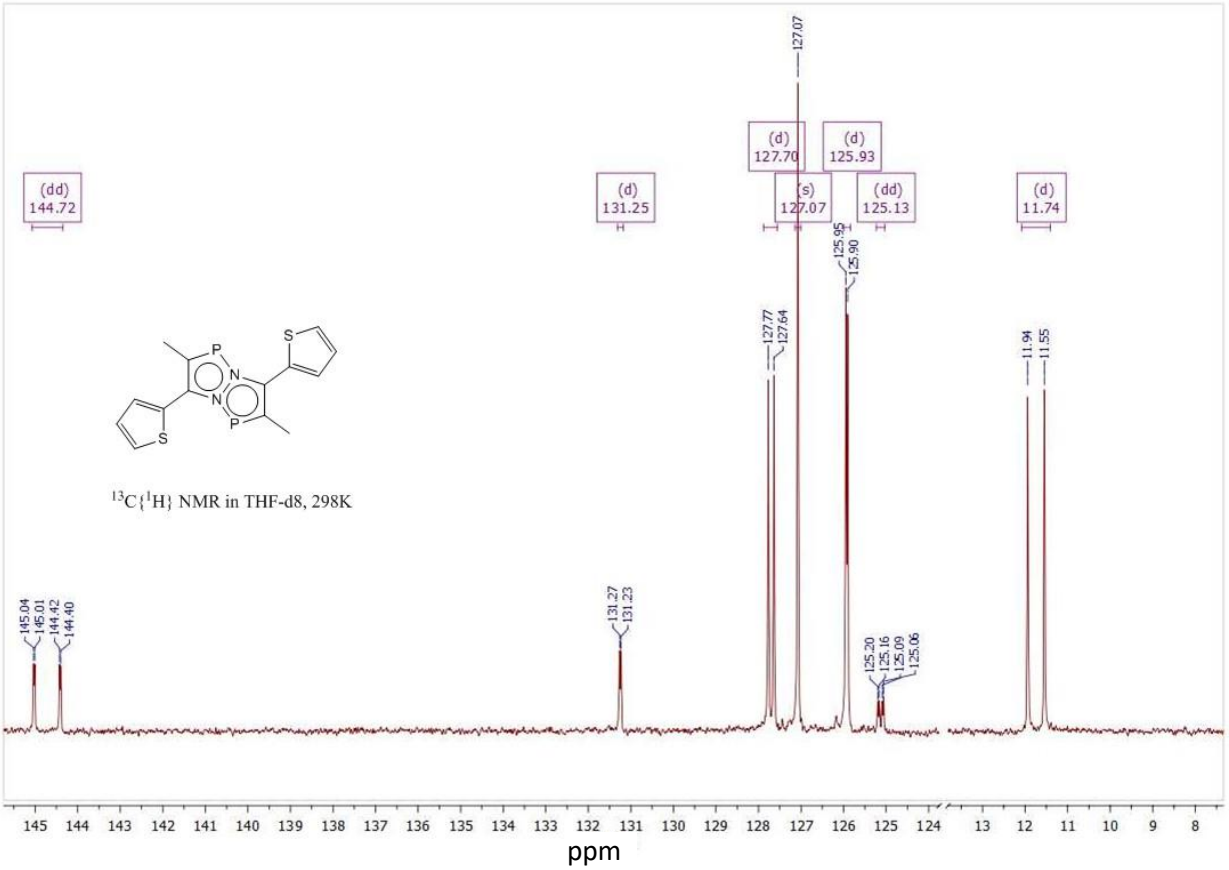

^{13}C{^{1}H} NMR in THF-d8, 298K

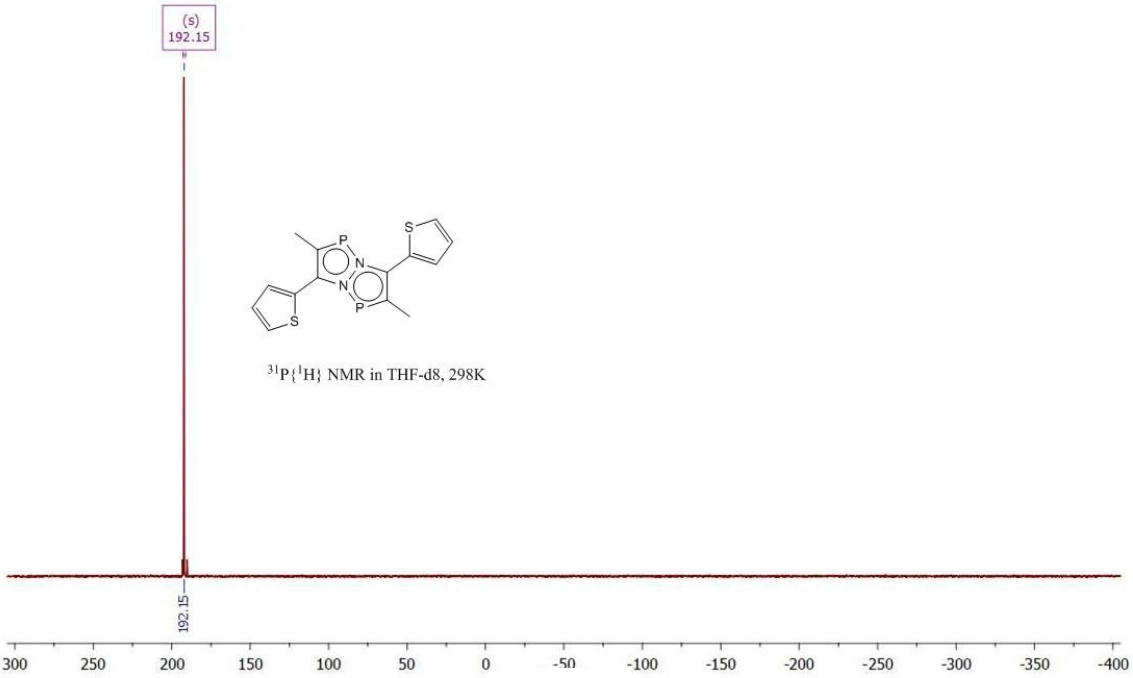

$^{31}P\{^{1}H\}$ NMR in THD-d8, 298K

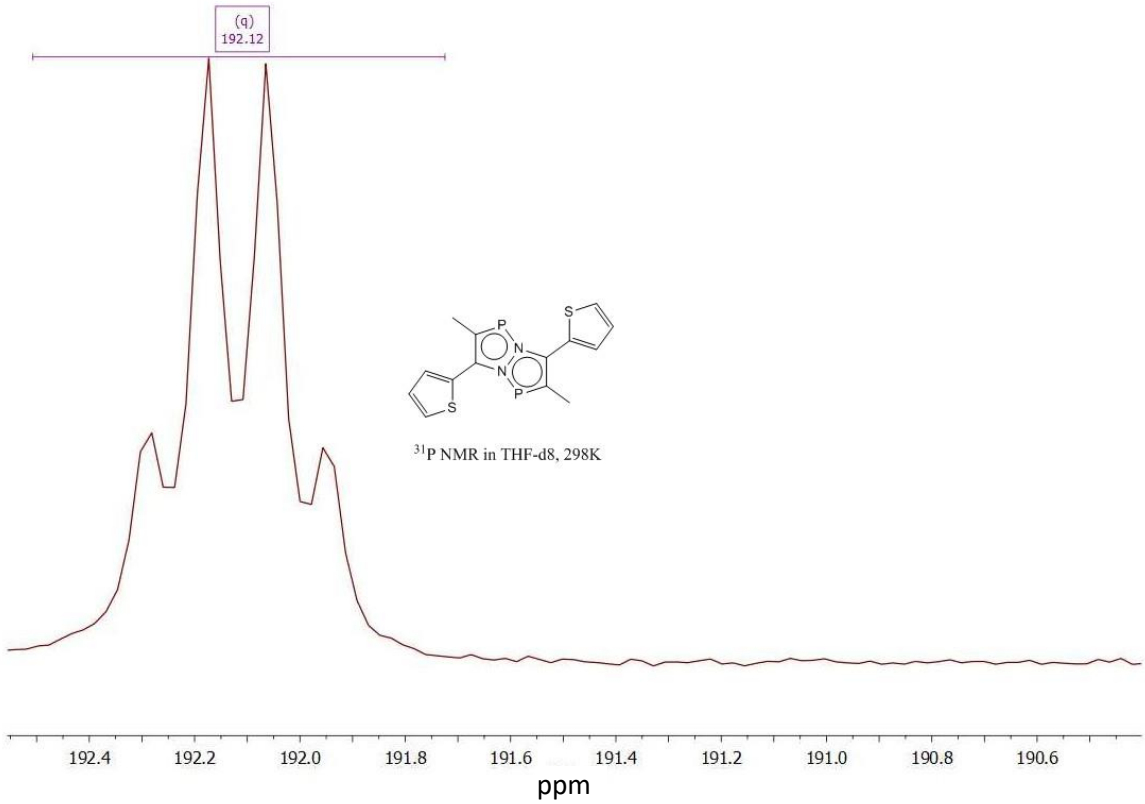

^{31}P NMR in THF-d8, 298K

Differential scanning calorimetry.

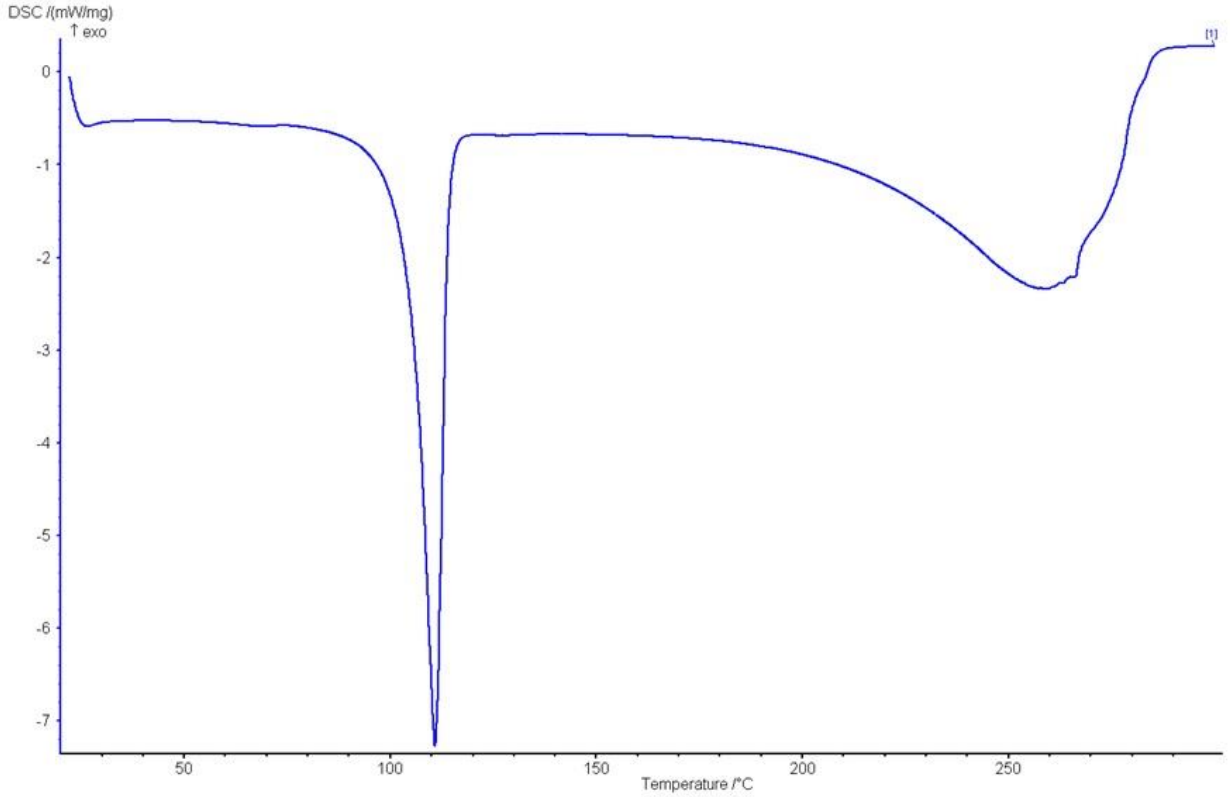

Figure S13. Differential scanning calorimetry of **5**.

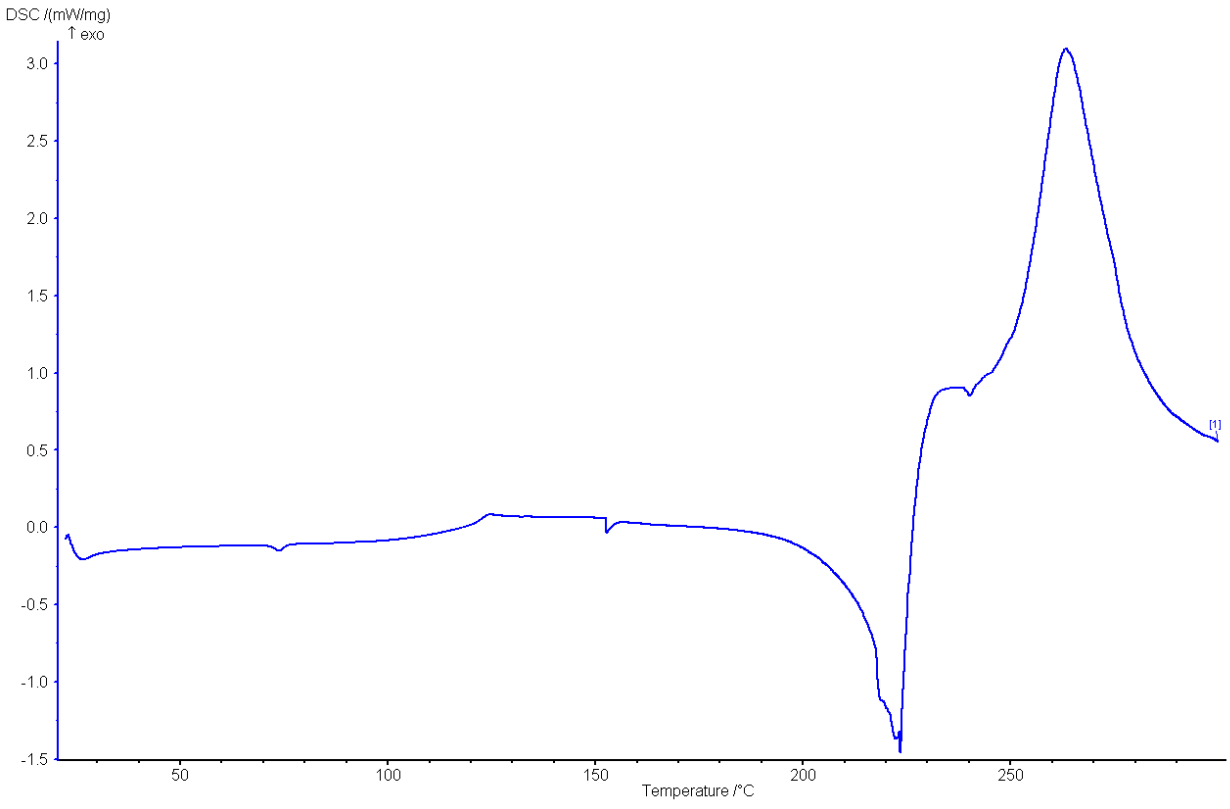

Figure S14. Differential scanning calorimetry of **6**.

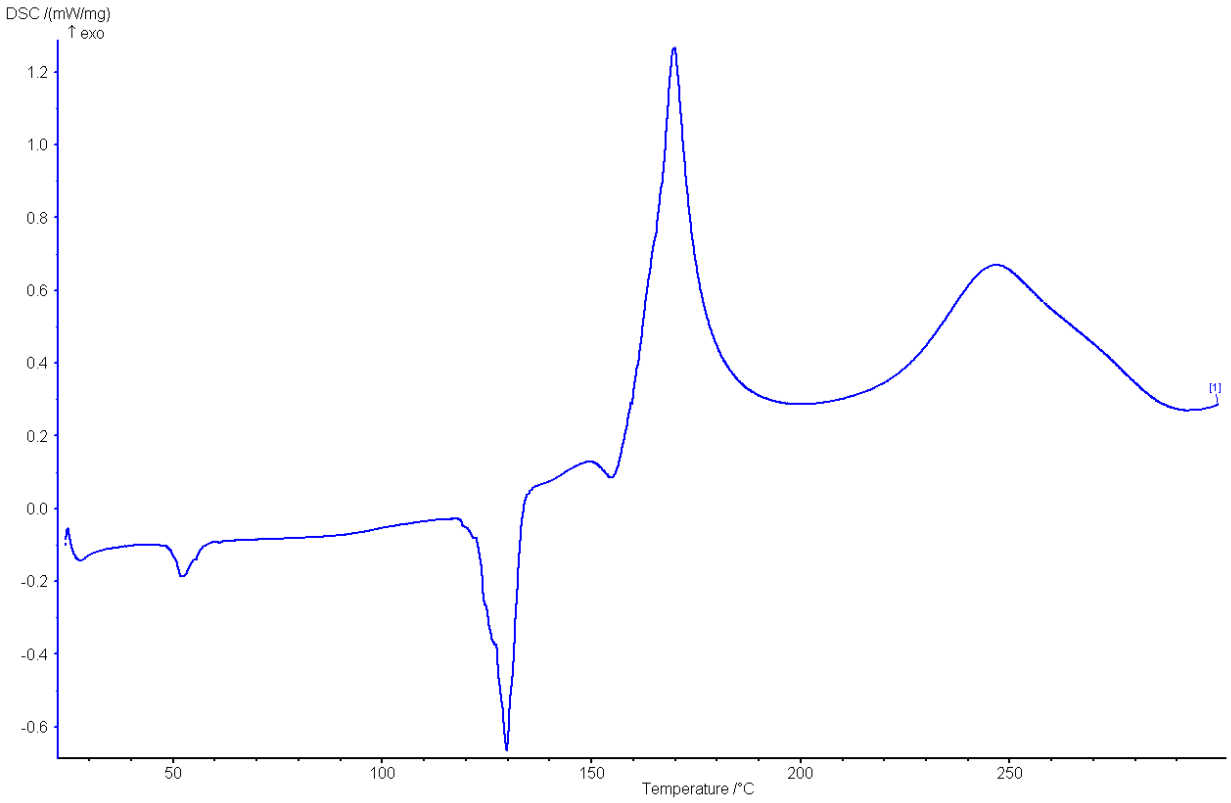

Figure S15. Differential scanning calorimetry of **7**.

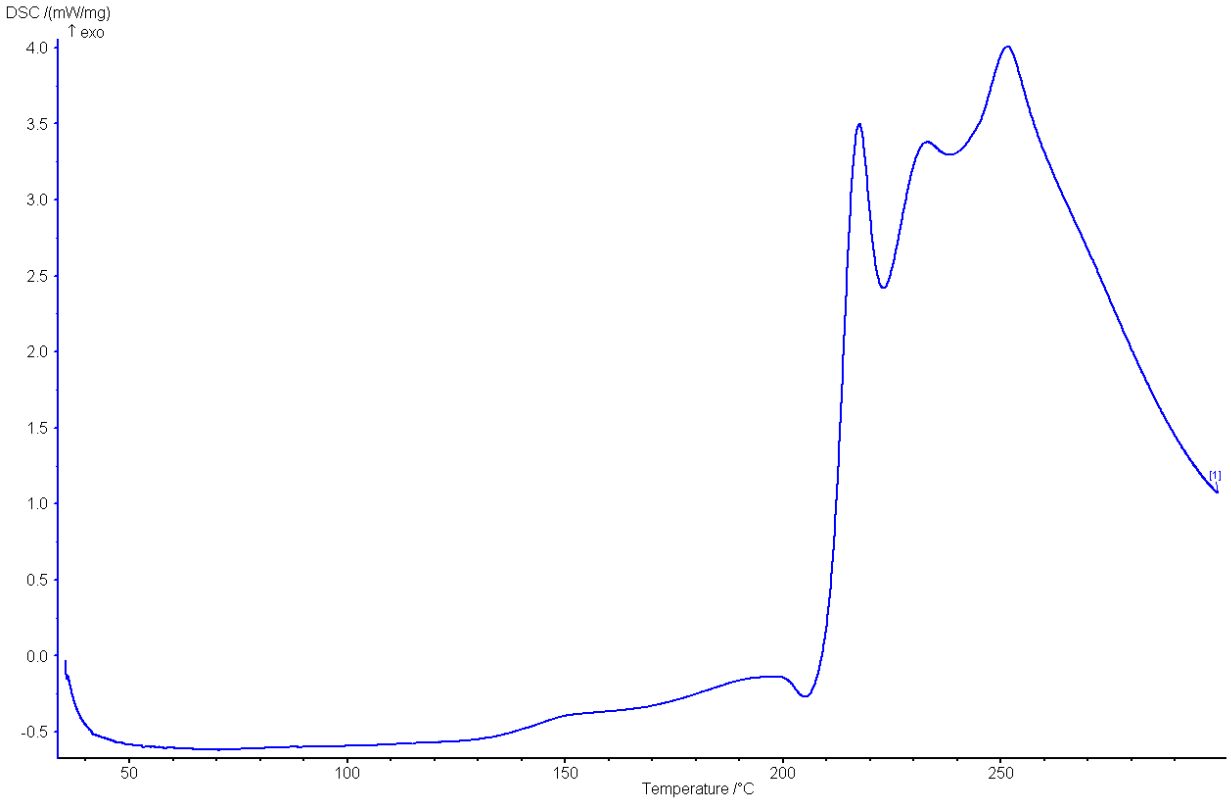

Figure S16. Differential scanning calorimetry of **8**.

Theoretical electron density

In order to obtain the theoretical electron density of **8** a single-point calculations were performed by DFT (B3LYP functional [S4-S6] with all electron 6-31G(d,p) basis sets [S7-S12] for all atoms via the Crystal17 program [S13] using experimental parameters of cells and crystals symmetry. The theoretical structural amplitudes ($\sin\theta/\lambda$ = 1.155 Å^{-1}) for **8** were calculated by the Crystal17 [S13]. Based on the calculated structural amplitudes, using the MoPro program [S14], the populations of the spherically symmetric valence shell (P_{val}), and the multipole parameters (P_{lm}) describing its deformation were obtained together with the corresponding expansion – contraction coefficients (k, k') for each of the complex atoms. The obtained values of P_{val}, P_{lm}, k and k' were used to construct the theoretical electron density. Analysis of topology of experimental–theoretical ρ(r) function was carried out using the WINXPRO program package [S15].

References

S1 *CrysAlis Pro Software System, Version 1.171.42.68a*, Rigaku Oxford Diffraction, 2022. Rigaku Corporation, Wroclaw, Poland.

S2 G. M. Sheldrick, *Acta Crystallogr.*, 2015, **A71**, 3.

S3 G. M. Sheldrick, *Acta Crystallogr.*, 2015, C**71**, 3.

S4 A. D. Becke, *J. Chem. Phys.*, 1993, **98**, 5648.

S5 C. Lee, W. Yang and R. G. Parr, *Phys. Rev.*, 1988, **37**, 785.

S6 P. J. Stephens, F. J. Devlin, C. F. Chabalowski and M. J. Frisch, *J. Phys. Chem.*, 1994, **98**, 11623.

S7 B. P. Pritchard, D. Altarawy, B. Didier, T. D. Gibson and T. L. Windus, *J. Chem. Inf. Model.*, 2019, **59**, 4814.

S8 R. Ditchfield, W. J. Hehre and J. A. Pople, *J. Chem. Phys.*, 1971, **54**, 724.

S9 M. M. Francl, W. J. Pietro, W. J. Hehre, J. S. Binkley, M. S. Gordon, D. J. DeFrees and J. A. Pople, *J. Chem. Phys.*, 1982, **77**, 3654.

S10 M. S. Gordon, J. S. Binkley, J. A. Pople, W. J. Pietro and W. J. Hehre, *J. Am. Chem. Soc.*, 1982, **104**, 2797.

S11 P. C. Hariharan and J. A. Pople, *Theor. Chim. Acta*, 1973, **28**, 213.

S12 W. J. Hehre, R. Ditchfield and J. A. Pople, *J. Chem. Phys.*, 1972, **56**, 2257.

S13 R. Dovesi, A. Erba, R. Orlando, C. M. Zicovich-Wilson, B. Civalleri, L. Maschio, M. Rérat, S. Casassa, J. Baima, S. Salustro and B. Kirtman, *Wiley Interdiscip. Rev.: Comput. Mol. Sci.*, 2018, **8**, e1360.

S14 C. Jelsch, B. Guillot, A. Lagoutte and C. Lecomte, *J. Appl. Crystallogr.*, 2005, **38**, 38.

S15 A. I. Stash and V. G. Tsirelson, *J. Appl. Crystallogr.*, 2014, **47**, 2086.